On the lifetimes of evaporating droplets

Final Version of PF#15-0634G

On the lifetimes of evaporating droplets with related initial and receding contact angles

Jutta M. Stauber,[1, a)] Stephen K. Wilson,[1, b)] Brian R. Duffy,[1, c)] and Khellil Sefiane[2, 3, d)]

[1)] *Department of Mathematics and Statistics, University of Strathclyde, Livingstone Tower, 26 Richmond Street, Glasgow, G1 1XH, United Kingdom*

[2)] *School of Engineering, University of Edinburgh, The King's Buildings, Mayfield Road, Edinburgh, EH9 3JL, United Kingdom*

[3)] *International Institute for Carbon-Neutral Energy Research (WPI-I2CNER), Kyushu University, 744 Motooka, Nishi-ku, Fukuoka 819-0395, Japan*

(Dated: 28th April 2015, revised 28th September and 21st October 2015)

A physically credible relationship based on the unbalanced Young force between the initial and receding contact angles of an evaporating droplet is proposed and used to give a complete description of the lifetime of a droplet evaporating in an idealised stick-slide mode. In particular, it is shown that the dependence of the lifetime on the initial contact angle is qualitatively different from that when the relationship between the initial and receding contact angles is not taken into account.

[a)]Email: jutta.stauber@strath.ac.uk

[b)]Author for correspondence. Email: s.k.wilson@strath.ac.uk

[c)]Email: b.r.duffy@strath.ac.uk

[d)]Email: k.sefiane@ed.ac.uk

I. INTRODUCTION

Droplet evaporation plays a crucial role in many practical applications (such as, for example, biochemical assays, deposition of DNA and RNA micro-arrays, deposition of pesticides, ink-jet printing, manufacture of novel optical and electronic materials, nano-wire fabrication, spray cooling, and thin film coating). As a result the evaporation of a fluid droplet on a solid substrate has been the subject of extensive theoretical and experimental investigations by a wide range of research groups from many different countries in recent years (see, for example, the recent review articles by Cazabat and Guéna[1], Erbil[2], Larson[3], and Lohse and Zhang[4]).

One aspect of droplet evaporation that has, until recently, received relatively little attention is that of the lifetime of a droplet (*i.e.* the time it takes for a droplet to evaporate entirely) and, in particular, how it depends on the manner in which it evaporates. This is rather surprising, since understanding and hence optimising the lifetime of an evaporating droplet could have considerable benefits in many of the practical applications mentioned above.

After a short transient in which it rapidly adjusts to a quasi-equilibrium shape with initial contact radius R_0 and initial contact angle θ_0, a droplet with initial volume V_0 deposited onto an ideal (*i.e.* perfectly smooth and chemically homogeneous) substrate at time $t = 0$ will, in principle, evaporate in the so-called "constant contact angle" (CA) mode in which the contact radius $R = R(t)$ and volume $V = V(t)$ decrease while the contact angle $\theta(t) = \theta_0$ remains constant. Of course, real substrates are never ideal, and so, in reality, the contact line of the droplet will be pinned by surface roughness and/or chemical heterogeneities for some or all of its lifetime. In the most extreme case in which the contact line always remains pinned, evaporation occurs in the so-called "constant contact radius" (CR) mode in which the contact angle $\theta = \theta(t)$ and volume $V = V(t)$ decrease while the contact radius $R(t) = R_0$ remains constant. As the pioneering studies of Picknett and Bexon[5] and Bourgès-Monnier and Shanahan[6] and many subsequent works have shown, in practice, the manner in which a droplet evaporates usually involves some combination of "stick" (*i.e.* with a pinned contact line) and "slide" (*i.e.* with a depinned contact line) phases. Note that we prefer to use the term "slide" rather than "slip" or "jump" to emphasise that, in general, the "stick" and "slide" phases can be of comparable duration.

A variety of "stick-slide" (SS) modes have been observed, but perhaps the most commonly reported (see, for example, the experiments described in references[6–14]) is one in which an initial stick phase is followed by a first slide phase with constant contact angle and a second

slide phase in which both the contact radius and the contact angle vary. In practice, the second slide phase can be relatively short compared to the other two phases, and so Nguyen and Nguyen[15], Dash and Garimella[14], and Stauber *et al.*[16] considered a simple but effective model for an idealised SS mode in which the second slide phase is entirely neglected and initially the droplet evaporates in a CR phase in which $R = R_0$ and $\theta(t)$ and $V(t)$ decrease until $\theta(t)$ reaches the receding contact angle θ^* ($0 \leq \theta^* \leq \theta_0$), at which the contact line depins and subsequently the droplet evaporates in a CA phase in which $\theta(t) = \theta^*$ and $R(t)$ and $V(t)$ decrease to zero at time $t = t_{\rm SS}$, where $t_{\rm SS}$ (which depends on both θ_0 and θ^*) denotes the lifetime of the droplet. This mode of evaporation is sketched in Figure 1. Stauber *et al.*[16] showed that the resulting theoretical predictions for $t_{\rm SS}$ are not, as might naively have been expected, always constrained to lie between the lifetimes of the extreme (*i.e.* the CR and CA) modes, and, moreover, that they are in good agreement with the lifetimes measured experimentally by previous authors. In order to make this latter comparison, the values of θ_0 and θ^* for each experiment (which, in general, depend of the nature of the substrate, the fluid and the atmosphere) were taken directly from the experimental measurements. However, it is expected that in practice the values of θ_0 and θ^* are related to each other, and so in the present work we extend the analysis of Stauber *et al.*[16] by proposing a physically credible relationship between them based on the unbalanced Young force and use this relationship to give a complete description of $t_{\rm SS}$. In particular, we show that the dependence of $t_{\rm SS}$ on θ_0 is qualitatively different from that when the relationship between θ_0 and θ^* is not taken into account.

II. THE MATHEMATICAL MODEL

A. The Diffusion-Limited Model

The diffusion-limited model employed in the present work is based on the assumption that the evaporation from the droplet is quasi-steady and limited by the diffusion of vapour in the quiescent atmosphere above it. This model, together with the assumption that the droplet is sufficiently small that gravitational effects can be neglected, is appropriate in a wide range of physical situations, and so has been used with considerable success by a large number of previous authors (see, for example, references[5,10,11,13,15–35]). The geometry of the mathematical model is shown in Figure 2. Referred to the cylindrical polar coordinates (r, z) shown in Figure

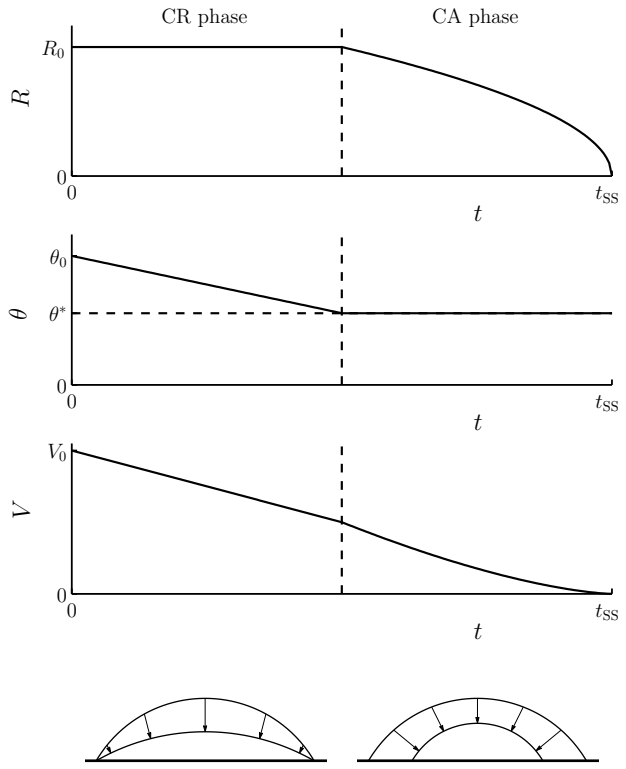

FIG. 1. Sketch of the idealised stick-slide (SS) mode studied in the present work in which initially the droplet evaporates in a CR phase in which $R = R_0$ and $\theta(t)$ and $V(t)$ decrease until $\theta(t)$ reaches the receding contact angle θ^* ($0 \leq \theta^* \leq \theta_0$), at which the contact line depins and subsequently the droplet evaporates in a CA phase in which $\theta(t) = \theta^*$ and $R(t)$ and $V(t)$ decrease to zero at time $t = t_{\rm SS}$.

2, the free surface of the droplet, $z = h(r,t)$, is a spherical cap with radius $\mathcal{R} = \mathcal{R}(t)$ ($\mathcal{R} \geq R$), contact radius $R = R(t)$ ($R \geq 0$), and contact angle $\theta = \theta(t)$ ($0 \leq \theta \leq \pi$) given by

$$h = -\mathcal{R}\cos\theta \pm \sqrt{\mathcal{R}^2 - r^2} \quad \text{where} \quad \mathcal{R} = \frac{R}{\sin\theta}. \tag{1}$$

Note that when $\pi/2 < \theta \leq \pi$ the physically relevant (*i.e.* the non-negative) part of h given by (1) is a double-valued function of r for $R \leq r < \mathcal{R}$, with the + and − signs corresponding to the upper and lower hemispheres, respectively. The volume of the droplet, V, is given by

$$V = 2\pi \int_0^R h\, r\, \mathrm{d}r = \frac{\pi R^3}{3} \frac{\sin\theta(2+\cos\theta)}{(1+\cos\theta)^2}, \tag{2}$$

and so, in particular, the initial volume, V_0, is given by

$$V_0 = \frac{\pi R_0^3}{3} \frac{\sin\theta_0(2+\cos\theta_0)}{(1+\cos\theta_0)^2}. \tag{3}$$

The concentration of vapour in the atmosphere, $c = c(r,z,t)$, satisfies Laplace's equation, $\nabla^2 c = 0$, subject to the boundary conditions that the atmosphere is saturated with vapour

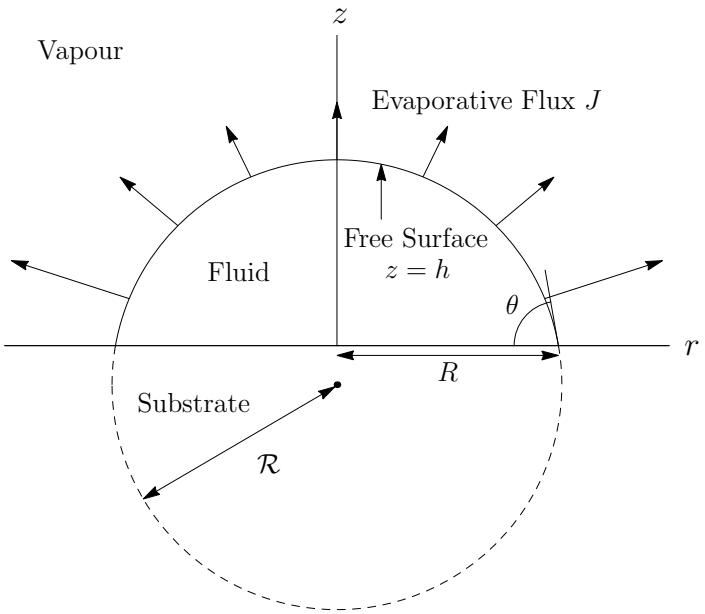

FIG. 2. Geometry of the mathematical model. The free surface of the droplet, $z = h$, is a spherical cap with radius $\mathcal{R}$, contact radius R, and contact angle θ. The arrows indicate the evaporative flux from the free surface of the droplet into the quiescent atmosphere above the droplet, J.

at the free surface of the droplet, *i.e.* $c = c_{\mathrm{sat}}$ on $z = h$, where c_{sat} denotes the saturation concentration, that the concentration of vapour approaches its ambient value far from the droplet, *i.e.* $c \to c_\infty$ as $r \to \infty$ for $z > 0$, where c_∞ ($0 \leq c_\infty \leq c_{\mathrm{sat}}$) denotes the ambient concentration, and that the substrate is impenetrable to vapour, *i.e.* $\partial c/\partial z = 0$ on $z = 0$ for $r > R$. In the simplest and most widely-used version of the model employed here, the saturation concentration c_{sat} is assumed to be constant, although in situations in which evaporative cooling can become significant (such as, for example, when the conductivity of the substrate is reduced, as studied by Dunn *et al.*[22], when the atmospheric pressure is reduced, as studied by Sefiane *et al.*[25], or when the contact angle becomes very large, as studied by Dash and Garimella[14]), the model can be extended to account for the temperature dependence of c_{sat}. As described by, for example, Popov[21], the solution for c when c_{sat} is constant was obtained by Lebedev[36], who solved a mathematically equivalent electrostatics problem. In particular, the evaporative flux from the free surface of the droplet, $J = J(r, t)$, defined by $J = -D\mathbf{n} \cdot \nabla c$, where $\mathbf{n}$ is the unit outward normal to the free surface and D is the diffusion coefficient of vapour in the atmosphere, is given by

$$J = \frac{D(c_{\mathrm{sat}} - c_\infty)}{R} \times \left[\frac{1}{2} \sin\theta + \sqrt{2}(\cosh\alpha + \cos\theta)^{3/2} \int_0^\infty \frac{\tau \cosh\theta\tau}{\cosh\pi\tau} \tanh\left[\tau(\pi - \theta)\right] P_{-1/2+i\tau}(\cosh\alpha)\, \mathrm{d}\tau \right], \quad (4)$$

where $P_{-1/2+i\tau}(\cosh\alpha)$ denotes the Legendre function of the first kind of degree $-1/2+i\tau$ and argument

$$\cosh\alpha = \frac{r^2\cos\theta \pm R\sqrt{R^2 - r^2\sin^2\theta}}{R^2 - r^2} \tag{5}$$

with the + and − signs again corresponding to the upper and lower hemispheres, respectively, when $\pi/2 < \theta \leq \pi$. In particular, the diffusion-limited model predicts that when $0 \leq \theta < \pi/2$ the flux is largest (theoretically integrably singular) at the contact line and smallest at the apex of the droplet (*i.e.* at $r = 0$), when $\theta = \pi/2$ the flux is uniform and given by $J = D(c_{\rm sat} - c_\infty)/R$, and when $\pi/2 < \theta \leq \pi$ the flux is largest at the apex of the droplet and smallest (theoretically zero) at the contact line (see, for example, Stauber *et al.*[35]).

B. The Evolution of the Droplet

Integrating the evaporative flux J given by (4) over the free surface of the droplet gives the total evaporative flux from the droplet at any instant, and hence (as described by, for example, Popov[21]) the rate of change of the volume of the droplet is given by

$$\frac{{\rm d}V}{{\rm d}t} = -\frac{\pi D(c_{\rm sat} - c_\infty)}{\rho}\frac{R\,g(\theta)}{(1+\cos\theta)^2}, \tag{6}$$

where the function $g = g(\theta)$ is defined by

$$g(\theta) = (1+\cos\theta)^2\left\{\tan\frac{\theta}{2} + 8\int_0^\infty \frac{\cosh^2\theta\tau}{\sinh 2\pi\tau}\tanh\left[\tau(\pi-\theta)\right]\,{\rm d}\tau\right\}. \tag{7}$$

As the droplet evaporates, R and θ evolve according to (6) with V given in terms of R and θ by (2). In particular, equation (6) determines the lifetime of the droplet, defined to be the time it takes for R and/or θ, and hence for V, to reach zero.

III. THE RELATIONSHIP BETWEEN θ_0 AND θ^*

In this Section we propose a relationship between θ_0 and θ^* based on the unbalanced Young force, specifically on the assumption that the scaled difference between the maximum pinning force and the initial pinning force is independent of both θ_0 and θ^*.

As we have already mentioned, a droplet deposited onto a substrate rapidly adjusts to a quasi-equilibrium shape with initial contact radius R_0 and initial contact angle θ_0. If the initial contact angle is equal to the receding contact angle, *i.e.* if $\theta_0 = \theta^*$, then the contact line immediately depins and thereafter the droplet simply evaporates in the CA mode with

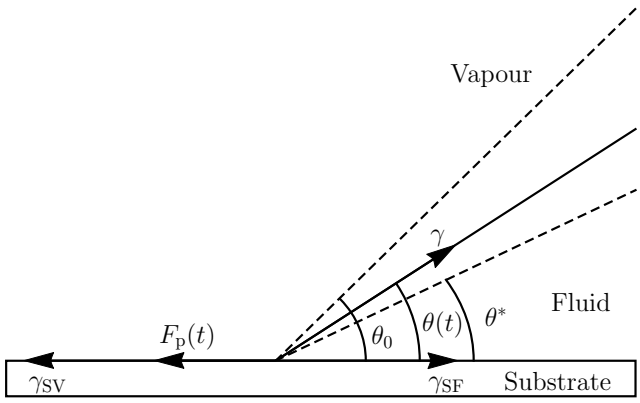

FIG. 3. Sketch of the contact line of an evaporating droplet with contact angle $\theta(t)$ showing the pinning force $F_\mathrm{p}(t)$. The dashed lines show the initial contact angle θ_0 and the receding contact angle θ^* when $\theta_0 > \theta^*$.

$\theta = \theta_0 = \theta^*$ constant and R decreasing. However, if the initial contact angle is greater than the receding contact angle, *i.e.* if $\theta_0 > \theta^*$, then, as sketched in Figure 3, the contact line is pinned by a pinning force per unit length $F_\mathrm{p} = F_\mathrm{p}(t)$ due to surface roughness and/or chemical heterogeneities of the substrate which opposes the unbalanced Young force, and the droplet begins to evaporate in a CR phase with $R = R_0$ constant and θ decreasing. Specifically, the horizontal force balance at the contact line reveals that F_p is given by

$$F_\mathrm{p}(t) = \gamma \cos(\theta(t)) + \gamma_\mathrm{SF} - \gamma_\mathrm{SV}, \tag{8}$$

where γ, γ_SV and γ_SF are the constant surface tensions of the fluid–vapour, substrate–vapour and substrate–fluid interfaces, respectively. Note that in the special case of an ideal substrate with no pinning force, *i.e.* in the special case $F_\mathrm{p} = 0$, equation (8) reduces to the well-known Young–Laplace equation for $\theta = \theta_0$. As the droplet continues to evaporate, θ decreases and hence F_p increases until it reaches its maximum possible value, denoted by $F_{\mathrm{p}\,\mathrm{max}}$, when $\theta = \theta^*$, at which instant the contact line depins and subsequently the droplet evaporates in a CA phase with $\theta = \theta^*$ constant and R decreasing. Subtracting the expression for the initial pinning force, $F_\mathrm{p}(0) = \gamma \cos\theta_0 + \gamma_\mathrm{SF} - \gamma_\mathrm{SV}$, from that for the maximum pinning force, $F_{\mathrm{p}\,\mathrm{max}} = \gamma \cos\theta^* + \gamma_\mathrm{SF} - \gamma_\mathrm{SV}$, gives a relationship between θ_0 and θ^*, namely

$$\cos\theta^* - \cos\theta_0 = f_\mathrm{p}, \tag{9}$$

where

$$f_\mathrm{p} = \frac{F_{\mathrm{p}\,\mathrm{max}} - F_\mathrm{p}(0)}{\gamma} \tag{10}$$

is the scaled difference between the maximum pinning force and the initial pinning force (hereafter simply referred to as the "maximum pinning force" for brevity). Note that, from

(9), physically realisable values of f_p lie in the range $0 \leq f_\mathrm{p} \leq 2$, with the extreme values $f_\mathrm{p} = 0$ and $f_\mathrm{p} = 2$ corresponding to the case $\theta_0 = \theta^*$ and to the case $\theta_0 = \pi$ and $\theta^* = 0$, respectively.

In general, the value of f_p as defined in (10) will depend on the nature of the substrate, the fluid and the atmosphere, and so could, in principle, depend on θ_0 and/or θ^*. However, in the present work we make the simplest possible assumption regarding f_p, namely that it is independent of both θ_0 and θ^*, and so (9) provides a simple explicit expression for θ^* in terms of θ_0 and f_p, namely

$$\theta^* = \max(0, \arccos(f_\mathrm{p} + \cos\theta_0)). \tag{11}$$

This physically credible relationship between θ_0 and θ^* is crucial to all of the results presented in the remainder of the present work, and so Figure 4 shows θ^* given by (11) plotted as a function of θ_0 for various values of f_p spanning the full range of physically realisable values, $0 \leq f_\mathrm{p} \leq 2$. For each value of f_p, the corresponding curve is symmetric about the line $\theta^* = \pi - \theta_0$, and intersects the θ_0-axis at the point $(\theta_{0\mathrm{min}}, 0)$ and the line $\theta_0 = \pi$ at the point $(\pi, \pi - \theta_{0\mathrm{min}})$, where $\theta_{0\mathrm{min}} = \arccos(1 - f_\mathrm{p})$. For values of θ_0 smaller than $\theta_{0\mathrm{min}}$ (*i.e.* when $0 \leq \theta_0 \leq \theta_{0\mathrm{min}}$) then (11) yields $\theta^* = 0$, so that the contact line never depins and the droplet evaporates in the CR mode, while for values of θ_0 larger than $\theta_{0\mathrm{min}}$ (*i.e.* when $\theta_{0\mathrm{min}} < \theta_0 \leq \pi$) then (11) yields $\theta^* = \arccos(f_\mathrm{p} + \cos\theta_0)$ $(0 < \theta^* \leq \pi - \theta_{0\mathrm{min}})$, and the droplet evaporates in the SS mode.

Stauber *et al.*[16] (Figure 2) showed that the theoretical predictions of the present model are in rather good agreement with the lifetimes extrapolated from 29 sets of experimental data for droplets evaporating in an SS mode in which the second slide phase is smaller than 10% of the lifetime of the droplet (so that the present idealised SS mode is likely to be an appropriate description of their behaviour) obtained by previous authors. Details of these sets of experimental data are given in Table 1. In order to make this comparison, the values of θ_0 and θ^* for each experiment (not given by Stauber *et al.*[16], and so given in Table 1 for reference) were taken directly from the experimental measurements. In particular, in the context of the present work, this is equivalent to determining the value of f_p for each experiment directly from the experimental measurements, and these values of f_p (calculated from the corresponding values of θ_0 and θ^* using (9)) are given in Table 1 for reference.

Reference	Fluid	Substrate	θ_0	θ^*	f_p
Bourgès-Monnier and	Water	Polished epoxy resin	0.97	0.44	0.34
Shanahan[6]	Water	Polished epoxy resin	1.04	0.26	0.46
Uno *et al.*[7]	Latex dispersion	$ODTES_{100}$ on glass	1.83	1.66	0.17
Fukai *et al.*[8]	Water	SO_3H on silicon	0.87	0.56	0.20
	Water	SO_3H on silicon	0.85	0.52	0.21
	Xylene	R_f on silicon	1.19	1.10	0.08
Li *et al.*[9]	Water	Dialkyl disulfides on	1.80	1.72	0.08
		gold-covered mica	1.44	1.31	0.13
			1.55	1.30	0.25
			1.31	1.20	0.11
			1.21	0.95	0.23
			1.14	0.95	0.17
			0.93	0.66	0.19
			0.78	0.57	0.13
			0.61	0.21	0.16
Song *et al.*[10]	Water	Platinum	1.61	1.41	0.20
Nguyen *et al.*[11]	Water	Oct-silicon	0.93	0.53	0.27
			0.93	0.57	0.25
			0.95	0.55	0.28
			0.92	0.56	0.24
	Water	Oct-silicon	0.96	0.65	0.23
	Water	OTS-silicon	1.81	1.64	0.16
	Water	Teflon	1.88	1.61	0.27
Lim *et al.*[12]	Water	Pyrex glass	1.14	0.67	0.36
	Diethylene glycol	Pyrex glass	0.68	0.37	0.15
	with coffee particles				
Yu *et al.*[13]	Water	Teflon on PDMS on glass	2.01	1.90	0.10
Dash and	Water	Teflon on silicon	2.14	1.99	0.13
Garimella[14]			2.12	1.96	0.14
			2.08	1.93	0.14

TABLE I. Details of the 29 sets of experimental data for droplets evaporating in an SS mode in which the second slide phase is smaller than 10% of the lifetime of the droplet obtained by previous authors and used in Figures 7 and 8. The values of θ_0 and θ^* were taken directly from the experimental measurements and the values of f_p were calculated from them using (9). In the "Substrate" column, "$ODTES_{100}$" denotes octadecyltriethoxysilane with a static contact angle of roughly 100° for pure water, "SO_3H" denotes 3-mercaptopropyltrimethoxysilane, "R_f" denotes perfluorohexylethyltrimethoxysilane, "Oct-silicon" denotes silicon hydrophobised with octanol, "OTS-silicon" denotes silicon hydrophobised with n-octadecyltrichlorosilane in heptane, and "PDMS" denotes polydimethylsiloxane.

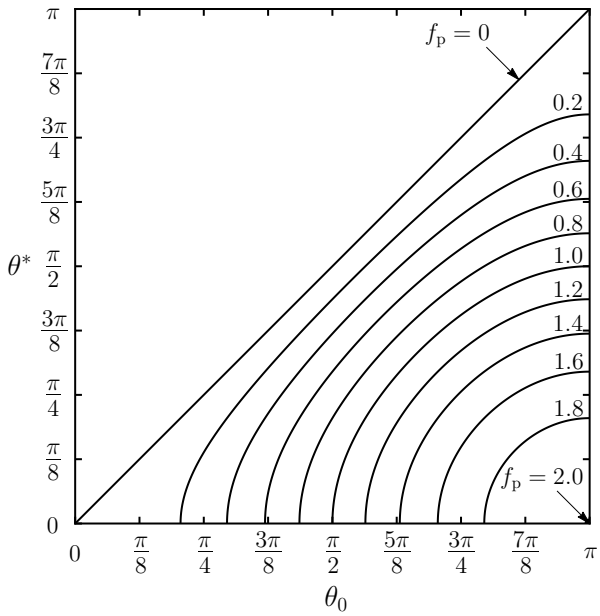

FIG. 4. The receding contact angle θ^* ($0 \leq \theta^* \leq \theta_0$) given by (11) plotted as a function of the initial contact angle θ_0 for various values of the maximum pinning force f_p spanning the full range of physically realisable values, $0 \leq f_\mathrm{p} \leq 2$, namely $f_\mathrm{p} = 0$, 0.2, 0.4, 0.6, 0.8, 1, 1.2, 1.4, 1.6, 1.8 and 2.

IV. THE LIFETIME OF AN EVAPORATING DROPLET

In this Section we use the relationship between θ_0 and θ^* given by (11) to determine how t_SS depends on θ_0 and f_p. In particular, we compare t_SS with the lifetimes of initially identical droplets (*i.e.* droplets with the same values of R_0 and θ_0, and hence of V_0) evaporating in the extreme modes for the full range of all possible initial contact angles, *i.e.* for $0 \leq \theta_0 \leq \pi$.

To simplify the subsequent presentation it is convenient to scale time t with the maximum lifetime of a droplet evaporating in the CA mode, namely

$$\frac{\rho}{2D(c_\mathrm{sat} - c_\infty)} \left(\frac{3V_0}{2\pi}\right)^{2/3} = \frac{\rho R_0^2}{2D(c_\mathrm{sat} - c_\infty)} \left(\frac{\sin\theta_0(2+\cos\theta_0)}{2(1+\cos\theta_0)^2}\right)^{2/3}. \tag{12}$$

With this scaling of time the lifetime of a droplet evaporating in the CR mode, denoted by $t_\mathrm{CR} = t_\mathrm{CR}(\theta_0)$, is given by

$$t_\mathrm{CR} = \left(\frac{2(1+\cos\theta_0)^2}{\sin\theta_0(2+\cos\theta_0)}\right)^{2/3} \int_0^{\theta_0} \frac{2\,\mathrm{d}\theta}{g(\theta)}, \tag{13}$$

and the lifetime of a droplet evaporating in the CA mode, denoted by $t_\mathrm{CA} = t_\mathrm{CA}(\theta_0)$, is given by

$$t_\mathrm{CA} = \left(\frac{2(1+\cos\theta_0)^2}{\sin\theta_0(2+\cos\theta_0)}\right)^{2/3} \frac{\sin\theta_0(2+\cos\theta_0)}{g(\theta_0)} \tag{14}$$

(see, for example, Stauber *et al.*[16]). Note that, as a consequence of the scaling (12), t_{CA} given by (14) attains its maximum value of unity at $\theta_0 = \pi/2$.

The lifetimes of droplets evaporating in the extreme modes given by (13) and (14) are, by definition, independent of θ^* and hence of f_{p}. However, as we have already seen, the lifetime of a droplet evaporating in the SS mode with θ^* given by (11) depends, in general, on f_{p} as well as on θ_0, *i.e.* $t_{\mathrm{SS}} = t_{\mathrm{SS}}(\theta_0, f_{\mathrm{p}})$.

If $0 \leq \theta_0 \leq \theta_{0\mathrm{min}}$, where $\theta_{0\mathrm{min}} = \arccos(1 - f_{\mathrm{p}})$, then $\theta^* = 0$, so that the droplet evaporates in the CR mode, and hence its lifetime is simply given by $t_{\mathrm{SS}} = t_{\mathrm{CR}}(\theta_0)$, where t_{CR} is given by (13).

If $\theta_{0\mathrm{min}} < \theta_0 \leq \pi$ then the droplet evaporates in the SS mode with $\theta^* = \arccos(f_{\mathrm{p}} + \cos\theta_0)$, and hence its lifetime is the sum of the duration of the CR phase (*i.e.* the time it takes for θ to decrease from θ_0 to θ^* with $R = R_0$) and the duration of the CA phase (*i.e.* the time it takes for R to decrease from $R = R_0$ to $R = 0$ with $\theta = \theta^*$), and hence is given by

$$t_{\mathrm{SS}} = \left(\frac{2(1+\cos\theta_0)^2}{\sin\theta_0(2+\cos\theta_0)}\right)^{2/3}\left[\int_{\theta^*}^{\theta_0}\frac{2\,\mathrm{d}\theta}{g(\theta)} + \frac{\sin\theta^*(2+\cos\theta^*)}{g(\theta^*)}\right] \tag{15}$$

(see, for example, Stauber *et al.*[16]). Note that (15) reduces to $t_{\mathrm{SS}} = t_{\mathrm{CR}}$ when $\theta^* = 0$, and so it is, in fact, valid for all values of θ_0.

Figure 5(a) shows t_{SS} given by (15) plotted as a function of θ_0 ($0 \leq \theta_0 \leq \pi$) for a range of values of f_{p}, together with the lifetimes of initially identical droplets evaporating in the extreme modes, t_{CR} and t_{CA}, given by (13) and (14), respectively. For clarity, Figure 5(b) shows the behaviour in the range $\pi/2 \leq \theta_0 \leq \pi$ in greater detail. Note that (as first pointed out by Picknett and Bexon[5]) the lifetimes (but not the evolutions) of the extreme modes coincide at $\theta_0 = \theta_{\mathrm{crit}} \simeq 2.5830$ where $t_{\mathrm{CR}} = t_{\mathrm{CA}} = t_{\mathrm{crit}} \simeq 0.9354$, and that (as described by Stauber *et al.*[35]) the extreme modes become indistinguishable in the limit $\theta_0 \to \pi^-$ and so, in particular, that $t_{\mathrm{SS}} = t_{\mathrm{CR}} = t_{\mathrm{CA}} = t_\pi = (4^{1/3}\log 2)^{-1} \simeq 0.9088$ at $\theta_0 = \pi$.

The most striking feature of Figure 5 is that the shapes of the curves representing t_{SS} are qualitatively different from those obtained by Stauber *et al.*[16] (Figures 3 and 4) in the case when θ_0 and θ^* are independent parameters. Specifically, as Figure 5 shows, whatever the value of f_{p}, the curves representing t_{SS} coincide with the curve representing t_{CR} for $0 \leq \theta_0 \leq \theta_{0\mathrm{min}}$, depart from it with vertical slope at $\theta_0 = \theta_{0\mathrm{min}}$ according to

$$t_{\mathrm{SS}} = t_{\mathrm{CR}} + \frac{2^{1/6}\pi(2-f_{\mathrm{p}})^{5/4}}{8 f_{\mathrm{p}}^{1/12}(3-f_{\mathrm{p}})^{2/3}}\sqrt{\theta_0 - \theta_{0\mathrm{min}}} + O\left(\theta_0 - \theta_{0\mathrm{min}}\right) \tag{16}$$

as $\theta_0 \to {\theta_{0\mathrm{min}}}^+$, increase to a local maximum at a value of θ_0 in the range $\pi/2 \leq \theta_0 \leq \pi$ (marked

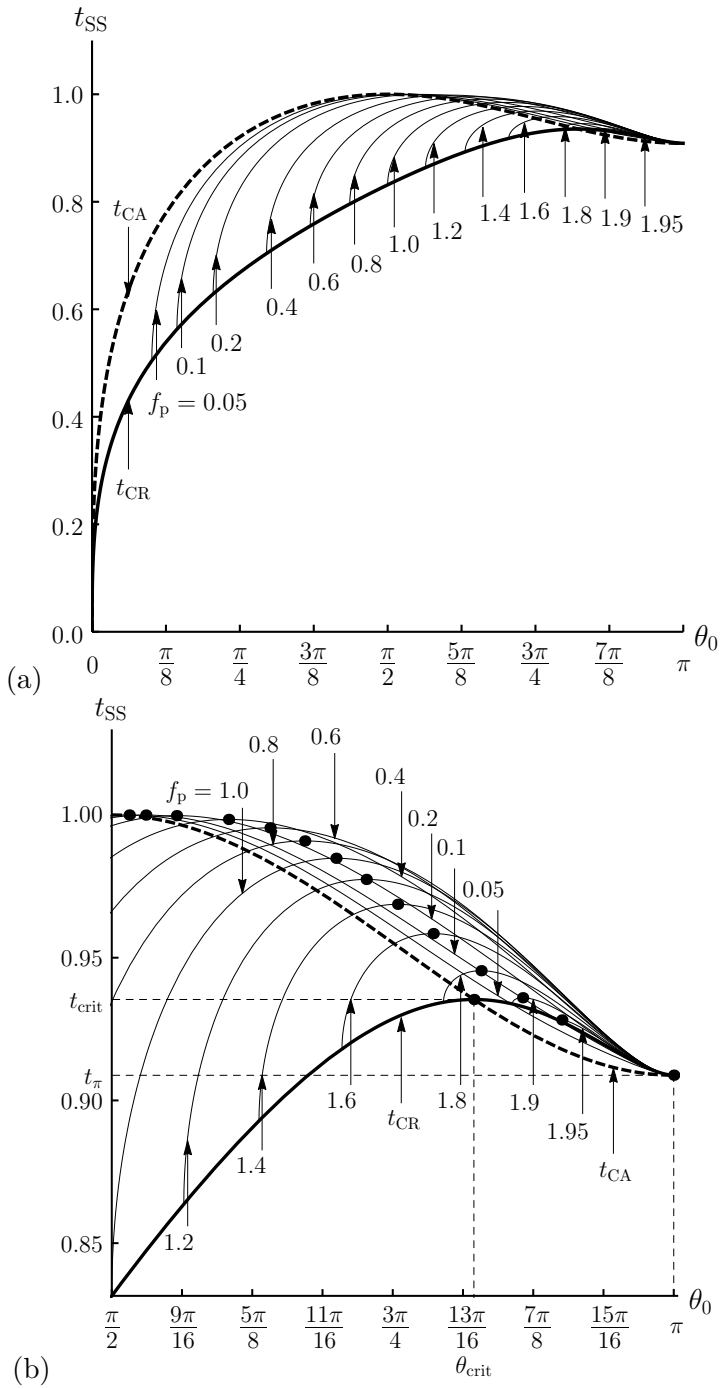

FIG. 5. (a) The lifetime of a droplet evaporating in the SS mode, t_{SS}, given by (15) plotted as a function of the initial contact angle θ_0 ($0 \leq \theta_0 \leq \pi$) for a range of values of the maximum pinning force, f_p, namely $f_p = 0.05$, 0.1, 0.2, 0.4, 0.6, 0.8, 1.0, 1.2, 1.4, 1.6, 1.8, 1.9 and 1.95, together with the lifetimes of initially identical droplets evaporating in the extreme modes, t_{CR} and t_{CA}, given by (13) and (14), respectively. Part (b) shows the behaviour in the range $\pi/2 \leq \theta_0 \leq \pi$ in greater detail. Note that $t_{SS} = t_{CR}(\theta_0)$ when $0 \leq \theta_0 \leq \theta_{0min}$, and that $t_{CR} = t_{CA} = t_{crit} \simeq 0.9354$ at $\theta_0 = \theta_{crit} \simeq 2.5830$ and $t_{SS} = t_{CR} = t_{CA} = t_\pi \simeq 0.9088$ at $\theta_0 = \pi$. In part (b) the local maximum of t_{SS}, which occurs at a value of θ_0 in the range $\pi/2 \leq \theta_0 \leq \pi$ and is also the global maximum of t_{SS} except when f_p lies in the range $1.9046 \leq f_p \leq 2$, is marked with a dot (•).

with a dot in Figure 5(b)) and then decrease, ultimately reaching the value $t_{\rm SS} = t_\pi$ with zero slope at $\theta_0 = \pi$. For contrast, recall that, unlike the present curves, the corresponding curves obtained by Stauber *et al.*[16] coincide with the curve representing $t_{\rm CA}$ (not $t_{\rm CR}$) when $0 \leq \theta_0 \leq \theta^*$ and depart from it with zero (not vertical) slope at $\theta_0 = \theta^*$. However, also recall that, like the present curves, the corresponding curves obtained by Stauber *et al.*[16] always lie below $t_{\rm CA}(\pi/2) = 1$ and always lie on or above the minimum of the two extreme modes (*i.e.* $t_{\rm SS} \geq \min(t_{\rm CR}, t_{\rm CA})$ for $0 \leq \theta_0 \leq \pi$), but may lie above the maximum of the two extreme modes when $\pi/2 < \theta_0 < \pi$. Moreover, the total envelope of the present curves as $f_{\rm p}$ varies between 0 and 2 is the same as the total envelope of the curves obtained by Stauber *et al.*[16] as θ^* varies between 0 and π.

As Figure 5 illustrates, in the limit $f_{\rm p} \to 0^+$ then $\theta_{0\rm min} \to 0^+$ and the curve representing $t_{\rm SS}$ approaches that representing $t_{\rm CA}$ from below for $0 < \theta_0 \leq \pi/2$ and from above for $\pi/2 < \theta_0 < \pi$ according to

$$t_{\rm SS} = t_{\rm CA} + \left(\frac{2(1+\cos\theta_0)^2}{\sin\theta_0(2+\cos\theta_0)}\right)^{2/3} \left(\frac{3 - 2\cos\theta_0 - 2\cos^2\theta_0}{g(\theta_0)\sin\theta_0} + \frac{g'(\theta_0)(2+\cos\theta_0)}{g^2(\theta_0)}\right) f_{\rm p} + O\left(f_{\rm p}^2\right), \tag{17}$$

where a dash ($'$) denotes differentiation with respect to argument. Furthermore, as Figure 5 also illustrates, in the limit $f_{\rm p} \to 2^-$ then $\theta_{0\rm min} \to \pi^-$ and the curve representing $t_{\rm SS}$ converges to that representing $t_{\rm CR}$ from above in the vanishingly small range $\theta_{0\rm min} < \theta_0 < \pi$. In addition, as Figure 5(b) illustrates, for most values of $f_{\rm p}$ the local maximum of $t_{\rm SS}$ is also its global maximum, but for values of $f_{\rm p}$ sufficiently close to 2 (specifically, for values of $f_{\rm p}$ in the range $1.9046 \leq f_{\rm p} \leq 2$) the global maximum of $t_{\rm SS}$ is $t_{\rm SS} = t_{\rm CR} = t_{\rm CA} = t_{\rm crit}$ at $\theta_0 = \theta_{\rm crit}$. As Figure 5(b) also illustrates, for most values of $f_{\rm p}$ the curves representing $t_{\rm SS}$ lie above the curve representing $t_{\rm CR}$ near $\theta_0 = \pi$, but for values of $f_{\rm p}$ in the range $0 \leq f_{\rm p} \leq f_{\rm p\,\pi}$, where $f_{\rm p\,\pi} \simeq 0.1520$, they lie below it (but still above the curve representing $t_{\rm CA}$).

In summary, Figure 5 shows that for sufficiently small values of θ_0 (*i.e.* for values in the range $0 \leq \theta_0 \leq \theta_{0\rm min}$) the droplet evaporates in the CR mode and has lifetime $t_{\rm SS} = t_{\rm CR}(\theta_0)$, while for larger values of θ_0 (*i.e.* for values in the range $\theta_{0\rm min} < \theta_0 \leq \pi$) the droplet evaporates in the SS mode and has lifetime $t_{\rm SS} = t_{\rm SS}(\theta_0, f_{\rm p})$ which is never less than both $t_{\rm CR}$ and $t_{\rm CA}$.

Note that the present curves are qualitatively much more similar (but still not identical) to that tentatively suggested by Shanahan *et al.*[37] than those obtained by Stauber *et al.*[16]. In particular, Shanahan *et al.*[37] used an ad hoc approximation to the diffusion-limited model (see Nguyen and Nguyen[29] for further discussion of this) and hypothesised the existence of

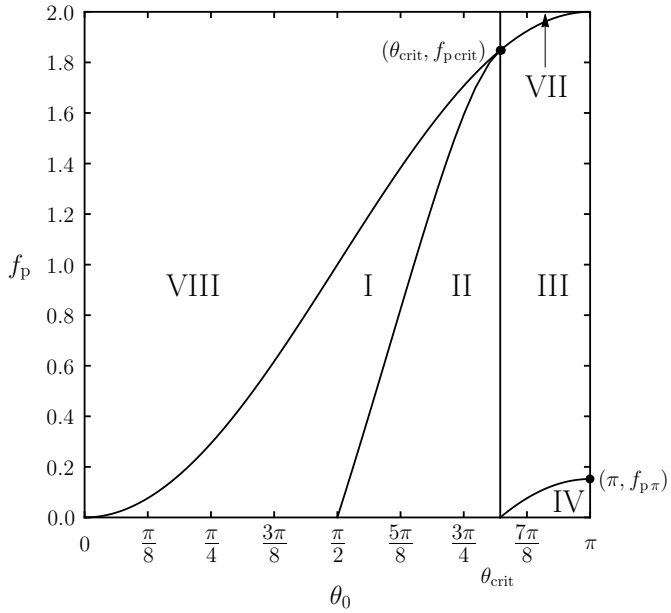

FIG. 6. Master diagram showing how the θ_0–f_p parameter plane is divided up into regions in which the six possible orderings of the lifetimes of initially identical droplets evaporating in the CR, CA and SS modes occur. Region I corresponds to $t_{CR} < t_{SS} < t_{CA}$, region II to $t_{CR} < t_{CA} < t_{SS}$, region III to $t_{CA} < t_{CR} < t_{SS}$, region IV to $t_{CA} < t_{SS} < t_{CR}$, region VII to $t_{CA} < t_{SS} = t_{CR}$, and region VIII to $t_{SS} = t_{CR} < t_{CA}$. In particular, note that $t_{SS} > \max(t_{CR}, t_{CA})$ in regions II and III. Note that regions I–IV, but not regions VII and VIII, appear in the corresponding diagram of Stauber *et al.*[16], and that regions V and VI found by Stauber *et al.*[16] do not appear here.

a sigmoidal curve representing "a transition between the two [extreme] regimes over a range of intermediate values of θ_0 [approximately $20^\circ \leq \theta_0 \leq 45^\circ$], corresponding to the change between pinning and (virtually) continuous triple line [*i.e.* contact line] recession" but that "its position, however, is not known". In particular, while the present curves depart from the curve representing t_{CR} at $\theta_0 = \theta_{0min}$ and cross the curve representing t_{CA} (albeit always at a value of θ_0 in the range $\pi/2 < \theta_0 < \pi$), they are not sigmoidal and have a considerably more complicated structure than that envisaged by Shanahan *et al.*[37].

V. MASTER DIAGRAM

Since the results presented in Figure 5 are fairly complicated, we follow the approach of Stauber *et al.*[16] (Figure 5) and summarise all of the possible relationships between the lifetimes of initially identical droplets evaporating in the CR, CA and SS modes in the master diagram shown in Figure 6, which shows how the θ_0–f_p parameter plane is divided up into regions in which the six possible orderings of t_{CR}, t_{CA} and t_{SS} occur. Four of these six regions, namely region I, which corresponds to $t_{CR} < t_{SS} < t_{CA}$, region II, which corresponds to

$t_{\rm CR} < t_{\rm CA} < t_{\rm SS}$, region III, which corresponds to $t_{\rm CA} < t_{\rm CR} < t_{\rm SS}$, and region IV, which corresponds to $t_{\rm CA} < t_{\rm SS} < t_{\rm CR}$, appear in the corresponding diagram of Stauber *et al.*[16], and so are labelled in the same way. The other two regions, namely region VII, which corresponds to $t_{\rm CA} < t_{\rm SS} = t_{\rm CR}$, and region VIII, which corresponds to $t_{\rm SS} = t_{\rm CR} < t_{\rm CA}$, correspond to $\theta^* = 0$ and hence collapse onto the θ_0-axis in the corresponding diagram of Stauber *et al.*[16] and so appear here for the first time. Similarly, two additional regions found by Stauber *et al.*[16], namely region V, which corresponds to $t_{\rm SS} = t_{\rm CA} < t_{\rm CR}$, and region VI which corresponds to $t_{\rm CR} < t_{\rm SS} = t_{\rm CA}$, correspond to $f_{\rm p} = 0$ and hence collapse onto the θ_0-axis in Figure 6 and so do not appear here. As Figure 6 shows, as $f_{\rm p}$ increases from 0 to 2, region IV disappears as $f_{\rm p}$ passes through the critical value $f_{\rm p\,\pi} \simeq 0.1520$, and regions I and II disappear and region VII appears as $f_{\rm p}$ passes through the critical value $f_{\rm p\,crit}$, where $f_{\rm p\,crit}$ is the value of $f_{\rm p}$ at which $\theta_{0\rm min} = \theta_{\rm crit}$, *i.e.* $f_{\rm p\,crit} = 1 - \cos(\theta_{\rm crit}) \simeq 1.8480$. In particular, Figure 6 confirms that $t_{\rm SS}$ is never less than both $t_{\rm CR}$ and $t_{\rm CA}$, and shows that regions I and IV (*i.e.* the regions in which $t_{\rm SS}$ lies between $t_{\rm CR}$ and $t_{\rm CA}$), regions II and III (*i.e.* the regions in which $t_{\rm SS}$ is greater than both $t_{\rm CR}$ and $t_{\rm CA}$), and regions VII and VIII (*i.e.* the regions in which $t_{\rm SS} = t_{\rm CA}$) all occupy substantial proportions of parameter space.

VI. DISCUSSION

In Sec. III we proposed a physically credible relationship between θ_0 and θ^* based on the assumption that $f_{\rm p}$ is independent of both θ_0 and θ^*, and in Secs IV and V we used it to give a complete description of the lifetime of a droplet evaporating in the idealised SS mode. In particular, we showed that the dependence of $t_{\rm SS}$ on θ_0 is qualitatively different from that described by Stauber *et al.*[16] when the relationship between θ_0 and θ^* is not taken into account, and is qualitatively much more similar (but still not identical) to that tentatively suggested by Shanahan *et al.*[37].

As we have already mentioned, in general, the value of $f_{\rm p}$ depends on the nature of the substrate, the fluid and the atmosphere. In the light of all this, what is most immediately striking about the values of $f_{\rm p}$ presented in Table 1 is how surprisingly similar they are, despite the fact that they are from different experiments by different authors on a variety of substrates with a range of surface roughnesses and chemical heterogeneities using several different fluids. In order to investigate this in more detail Figure 7 shows θ^* plotted as a function of θ_0 obtained from the 29 sets of experimental data listed in Table 1. Figure 7 also includes a solid curve

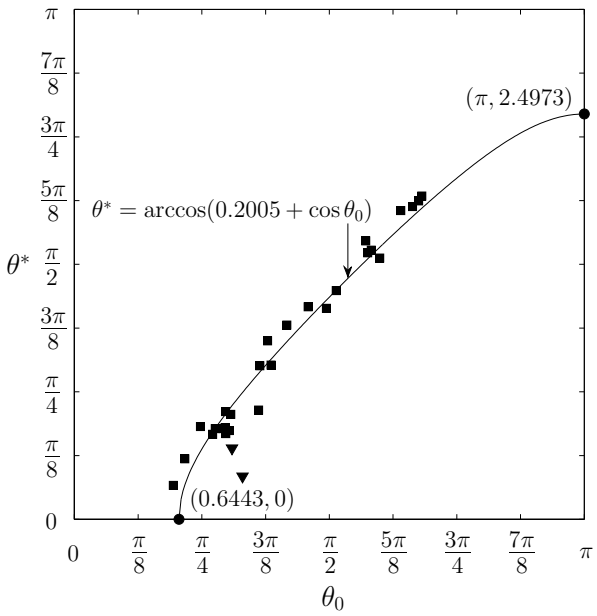

FIG. 7. The receding contact angle θ^* plotted as a function of the initial contact angle θ_0 obtained from the 29 sets of experimental data listed in Table 1. The values from the two experiments by Bourgès-Monnier and Shanahan[6] are denoted by inverted triangles (▼) rather than by squares (■). The solid curve shows the relationship (11) with the value of f_p that best fits all 29 sets of experimental data, namely $f_\mathrm{p} = 0.2005$.

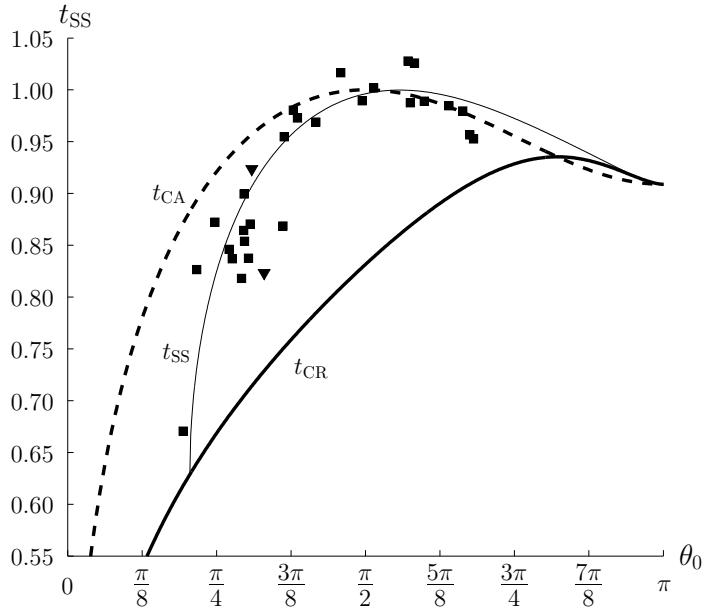

FIG. 8. The lifetimes of the droplets extrapolated from the 29 sets of experimental data listed in Table 1 plotted as a function of the initial contact angle θ_0. The lifetimes from the two experiments by Bourgès-Monnier and Shanahan[6] are denoted by inverted triangles (▼) rather than by squares (■). Also shown are the theoretical predictions for the lifetimes of initially identical droplets evaporating in the CR, CA and SS modes, t_{CR}, t_{CA} and t_{SS}, the latter calculated using $f_\mathrm{p} = 0.2005$.

showing the relationship (11) with the value of f_{p} that best fits all 29 sets of experimental data, namely $f_{\mathrm{p}} = 0.2005$. The corresponding value of $\theta_{0\mathrm{min}}$ is $\theta_{0\mathrm{min}} \simeq 0.6443 \simeq 37^{\circ}$, and hence the corresponding values of θ^* vary between $\theta^* = 0$ and $\theta^* = \pi - \theta_{0\mathrm{min}} \simeq 2.4973 \simeq 143^{\circ}$. The quality of the fit is confirmed by an R^2 value of $R^2 = 0.9676$, and by the fact that even if the two experiments by Bourgès-Monnier and Shanahan[6] with the largest known roughness values and two of the three largest values of f_{p} in Table 1 (denoted by inverted triangles rather than by squares in Figure 7) are excluded, then the value of f_{p} that best fits all of the remaining 27 sets of experimental data decreases only slightly to 0.1858 and the corresponding R^2 value rises only slightly to $R^2 = 0.9800$. Figure 8 shows the lifetimes of the droplets extrapolated from the 29 sets of experimental data listed in Table 1 plotted as a function of θ_0. Also shown are the theoretical predictions for the lifetimes of initially identical droplets evaporating in the CR, CA and SS modes, t_{CR}, t_{CA} and t_{SS}, the latter calculated using $f_{\mathrm{p}} = 0.2005$. In particular, Figure 8 shows that the theoretical prediction for t_{SS} using this single value of f_{p} is reasonably close to all 29 of the experimentally determined lifetimes (even those from the two experiments by Bourgès-Monnier and Shanahan[6]), and that it captures the qualitative behaviour of the experimental results surprisingly well. Despite this impressive level of agreement, we do not, of course, seek to claim that this single value of f_{p} will be appropriate in all situations. Rather, we simply wish to point out that the unexpected insensitivity of the experimentally determined lifetimes to the surface roughness and chemical heterogeneity of the substrates revealed in the present work highlights the need for further theoretical and experimental work on the nature of contact line pinning and depinning on non-ideal substrates.

ACKNOWLEDGEMENTS

The first author (JMS) gratefully acknowledges the financial support of the United Kingdom Engineering and Physical Science Research Council (EPSRC), the University of Strathclyde, and the University of Edinburgh via a postgraduate research studentship. This work was undertaken while the second author (SKW) was a Leverhulme Trust Research Fellow (2013–16) supported by award RF-2013-355 "Small Particles, Big Problems: Understanding the Complex Behaviour of Nanofluids".

REFERENCES

[1]A.-M. Cazabat and G. Guéna, "Evaporation of macroscopic sessile droplets," Soft Matter **6**, 2591–2612 (2010).

[2]H.Y. Erbil, "Evaporation of pure liquid sessile and spherical suspended drops: a review," Adv. Coll. Int. Sci. **170**, 67–86 (2012).

[3]R.G. Larson, "Transport and deposition patterns in drying sessile droplets," AIChE J. **60** 1538–1571 (2014).

[4]D. Lohse and X. Zhang, "Surface nanobubbles and nanodroplets," Rev. Mod. Phys. **87** 981–1035 (2015).

[5]R.G. Picknett and R. Bexon, "The evaporation of sessile or pendant drops in still air," J. Coll. Int. Sci. **61**, 336–350 (1977).

[6]C. Bourgès-Monnier and M.E.R. Shanahan, "Influence of evaporation on contact angle," Langmuir **11**, 2820–2829 (1995).

[7]K. Uno, K. Hayashi, T. Hayashi, K. Ito, and H. Kitano, "Particle adsorption in evaporating droplets of polymer latex dispersions on hydrophilic and hydrophobic surfaces," Coll. Polym. Sci. **276**, 810–815 (1998).

[8]J. Fukai, H. Ishizuka, Y. Sakai, M. Kaneda, M. Morita, and A. Takahara, "Effects of droplet size and solute concentration on drying process of polymer solution droplets deposited on homogeneous surfaces," Int. J. Heat Mass Trans. **49**, 3561–3567 (2006).

[9]G. Li, S.M. Flores, C. Vavilala, M. Schmittel, and K. Graf, "Evaporation dynamics of microdroplets on self-assembled monolayers and dialkyl disulfides," Langmuir **25**, 13438–13447 (2009).

[10]H. Song, Y. Lee, S. Jin, H.-Y. Kim, and J.Y. Yoo, "Prediction of sessile drop evaporation considering surface wettability," Microelec. Eng. **88**, 3249–3255 (2011).

[11]T.A.H. Nguyen, A.V. Nguyen, M.A. Hampton, Z.P. Xu, L. Huang, and V. Rudolph, "Theoretical and experimental analysis of droplet evaporation on solid surfaces," Chem. Eng. Sci. **69**, 522–529 (2012).

[12]T. Lim, J. Yang, S. Lee, J. Chung, and D. Hong, "Deposit pattern of inkjet printed pico-liter droplet," Int. J. Precis. Eng. Manufact. **13**, 827–833 (2012).

[13]Y.-S. Yu, Z. Wang, and Y.-P. Zhao, "Experimental and theoretical investigations of evaporation of sessile water droplet on hydrophobic surfaces," J. Coll. Int. Sci. **365**, 254–259 (2012).

[14]S. Dash and S.V. Garimella, "Droplet evaporation dynamics on a superhydrophobic surface with negligible hysteresis," Langmuir **29**, 10785–10795 (2013).

[15]T.A.H. Nguyen and A.V. Nguyen, "Increased evaporation kinetics of sessile droplets by using nanoparticles," Langmuir **28**, 16725–16728 (2012).

[16]J.M. Stauber, S.K. Wilson, B.R. Duffy, and K. Sefiane, "On the lifetimes of evaporating droplets," J. Fluid Mech. **744**, R2 (2014).

[17]R.D. Deegan, O. Bakajin, T.F. Dupont, G. Huber, S.R. Nagel, and T.A. Witten, "Capillary flow as the cause of ring stains from dried liquid drops," Nature **389**, 827–829 (1997).

[18]R.D. Deegan, O. Bakajin, T.F. Dupont, G. Huber, S.R. Nagel, and T.A. Witten, "Contact line deposits in an evaporating drop," Phys. Rev. E **62**, 756–765 (2000).

[19]H.Y. Erbil, G. McHale, and M.I. Newton, "Drop evaporation on solid surfaces: constant contact angle mode," Langmuir **18**, 2636–2641 (2002).

[20]H. Hu and R.G. Larson, "Evaporation of a sessile droplet on a substrate," J. Phys. Chem. B **106**, 1334–1344 (2002).

[21]Y.O. Popov, "Evaporative deposition patterns: spatial dimensions of the deposit," Phys. Rev. E **71**, 036313 (2005).

[22]G.J. Dunn, S.K. Wilson, B.R. Duffy, S. David, and K. Sefiane, "The strong influence of substrate conductivity on droplet evaporation," J. Fluid Mech. **623**, 329–351 (2009).

[23]G.J. Dunn, S.K. Wilson, B.R. Duffy, S. David, and K. Sefiane, "Evaporation of a thin droplet on a thin substrate with a high thermal resistance," Phys. Fluids **21**, 052101 (2009).

[24]H. Masoud and J.D. Felske, "Analytical solution for inviscid flow inside an evaporating sessile drop," Phys. Rev. E **79**, 016301 (2009).

[25]K. Sefiane, S.K. Wilson, S. David, G.J. Dunn, and B.R. Duffy, "On the effect of the atmosphere on the evaporation of sessile droplets of water," Phys. Fluids **21**, 062101 (2009).

[26]J. Eggers and L.M. Pismen, "Nonlocal description of evaporating drops," Phys. Fluids **22**, 112101 (2010).

[27]H. Gelderblom, Á.G. Marín, H. Nair, A. van Houselt, L. Lefferts, J.H. Snoeijer, and D. Lohse, "How water droplets evaporate on a superhydrophobic substrate," Phys. Rev. E **83**, 026306 (2011).

[28]H. Gelderblom, O. Bloemen, and J.H. Snoeijer, "Stokes flow near the contact line of an evaporating drop," J. Fluid Mech. **709**, 69–84 (2012).

[29]T.A.H. Nguyen and A.V. Nguyen, "On the lifetime of evaporating sessile droplets," Langmuir **28**, 1924–1930 (2012).

[30]B. Sobac and D. Brutin, "Thermal effects of the substrate on water droplet evaporation," Phys. Rev. E **86**, 021602 (2012).

[31]E.L. Talbot, A. Berson, P.S. Brown, and C.D. Bain, "Evaporation of picoliter droplets of surfaces with a range of wettabilities and thermal conductivities," Phys. Rev. E **85**, 061604 (2012).

[32]S. Dash and S.V. Garimella, "Droplet evaporation on heated hydrophobic and superhydrophobic surfaces," Phys. Rev. E **89**, 042402 (2014).

[33]T.A.H. Nguyen and A.V. Nguyen, "Transient volume of evaporating sessile droplets: 2/3, 1/1, or another power law?" Langmuir **30**, 6544–6547 (2014).

[34]S. Semenov, A. Trybala, R.G. Rubio, N. Kovalchuk, V.(M.) Starov, and M.G. Velarde, "Simultaneous spreading and evaporation: recent developments," Adv. Coll. Int. Sci. **206**, 382–398 (2014).

[35]J.M. Stauber, S.K. Wilson, B.R. Duffy, and K. Sefiane, "The evaporation of droplets on strongly hydrophobic substrates," Langmuir **31**, 3653–3660 (2015).

[36]N.N. Lebedev, *Special Functions and Their Applications* (Prentice Hall Inc., 1965).

[37]M.E.R. Shanahan, K. Sefiane, and J.R. Moffat, "Dependence of volatile droplet lifetime on the hydrophobicity of the substrate," Langmuir **27**, 4572–4577 (2011).